Comparison of Particle-In-Cell Simulations with Experimentally Observed Frequency Shifts Between Ions of the Same Mass-To-Charge in Fourier Transform Ion Cyclotron Resonance Mass Spectrometry

Franklin E. Leach III,[a] Andriy Kharchenko,[b] Ron M. A. Heeren,[b] Eugene Nikolaev,[c] and I. Jonathan Amster[a]

[a] Department of Chemistry, University of Georgia, Athens, Georgia, USA
[b] FOM Institute for Atomic and Molecular Physics, Amsterdam, The Netherlands
[c] The Institute for Energy Problems of Chemical Physics, Moscow, Russia

It has been previously observed that the measured frequency of ions in a Fourier transform mass spectrometry experiment depend upon the number of trapped ions, even for populations consisting exclusively of a single mass-to-charge. Since ions of the same mass-to-charge are thought not to exert a space–charge effect among themselves, the experimental observation of such frequency shifts raises questions about their origin. To determine the source of such experimentally observed frequency shifts, multiparticle ion trajectory simulations have been conducted on monoisotopic populations of Cs^+ ranging from 10^2 ions to 10^6 ions. A close match to experimental behavior is observed. By probing the effect of ion number and orbital radius on the shift in the cyclotron frequency, it is shown that for a monoisotopic population of ions, the frequency shift is caused by the interaction of ions with their image-charge. The addition of ions of a second mass-to-charge to the simulation allows the comparison of the magnitude of the frequency shift resulting from space–charge (ion–ion) effects versus ion interactions with their image charge. (J Am Soc Mass Spectrom 2010, 21, 203–208) © 2010 Published by Elsevier Inc. on behalf of American Society for Mass Spectrometry

Fourier transform ion cyclotron resonance mass spectrometry (FTICR-MS) [1] provides the highest mass accuracy and highest mass resolution of any currently available mass spectrometer. The cyclotron motion of an ion arises due to a radially constraining magnetic field and the frequency of this motion can be defined as:

$$\omega_c = qB/m \quad (1)$$

where B is the magnetic field, q is the ion's charge, and m is the ion's mass. Values of cyclotron frequency ($\omega_c/2\pi$) range from tens of kHz to MHz for most ions. In practice, the magnitude of the observed cyclotron frequency is slightly reduced by the radially-repulsive trapping electric field, and to a lesser degree, by the repulsive electric field that exists between ions of like charge, also known as space–charge. The study of deviations from the expected cyclotron frequency has been of continuing interest in FTICR-MS [2–9] as the desire to reduce mass errors to the sub-ppm range has increased. These ion population-dependent shifts are small in magnitude, corresponding to shifts of several Hz to less than 1 Hz. For example, a shift of 0.1 Hz for an ion of *m/z* 500 at 7.0 T corresponds to 0.47 ppm in mass measurement error. These differences in measured frequency are due to space charge interactions in the FTICR analyzer cell [10, 11] as well as image-charge interactions [12].

Recently, our laboratory has made an experimental investigation of frequency shifts amongst monoisotopic populations of Cs^+ ions [13] and attributed the source of these shifts to space charge interaction between like ions. These findings contradict previous theoretical studies of space charge interactions of ions contained within a Penning trap, where like ions have been proposed to have no coulombic effect on cyclotron frequency [2, 12]. Although coulombic interactions can be investigated in the laboratory, the experimental approach is limited by the inability to precisely know the number of ions present in the analyzer cell or their spatial distribution. In contrast, computational simulations provide the means to specify the number of ions present in the analyzer, as well as their mass, charge, and spatial distribution. Multiparticle simulations can be used to examine ion motion in FTICR-MS as a function of the above-mentioned parameters and to

Address reprint requests to Dr. I. J. Amster, Department of Chemistry, University of Georgia, Athens, GA 30602-2556, USA. E-mail: jamster@uga.edu

1044-0305/10/$32.00
doi:10.1016/j.jasms.2009.10.001

Published online October 6, 2009
Received June 30, 2009
Revised September 30, 2009
Accepted October 2, 2009

determine the root causes of frequency shifts for a monoisotopic population of ions.

To gain insight into ion motion in the presence of applied electric and magnetic fields it is possible to utilize a commercially available software package, such as SIMION [14], but this approach is limited to the motion of tens of ions, whereas typical experimental populations range from 10^3 to 10^6, and does not incorporate ion–ion interaction nor ion–image charge interaction. A SIMION model has recently been developed which incorporates ion–image charge detection, but does not include the forces of the coulombic interactions [15]. Particle–particle methods can be applied to account for ion–ion interaction and allow for the calculation of FTICR spectral line shapes as well as frequency shifts [16], but require very large computational resources [17].

The particle-in-cell (PIC) approach provides a computationally tractable method for simulating the ion motion of large populations of ions, with a realistic model for coulombic effects such as ion–ion and ion–image charge interactions [18–22]. Originally developed by the plasma physics community, particle-in-cell methods were first applied to ion trajectory simulations in FTICR-MS by Mitchell and Smith [23, 24] and subsequently Nikolaev et al. [25]. Using a PIC algorithm, a model has been developed to simulate prior experimental observations in our laboratory. As shown below, these simulations reveal the source of observed frequency shifts to be due to interactions between ions and their image charge induced in the surrounding electrodes.

Experimental

Multiparticle ion trajectory simulations were conducted on Linux clusters located at the University of Georgia and the Foundation for Fundamental Research on Matter-Institute for Atomic and Molecular Physics (FOM-AMOLF) using a serial version of the PIC code and parameters summarized in Table 1. A monoisotopic Cs^+ (*m/z* 132.9054, z = 1) population was varied in ion number from 10^2 to 10^6 while constrained radially by a magnetic field of 7.0 T and trapped axially by 1 V. A cubic trapping potential and an idealized quadrupolar trapping potential of a Penning trap were employed using particle-in-cell methods to enable coulombic interactions. The analyzer geometry in all simulations was 5.08 cm × 5.08 cm × 5.08 cm, corresponding to a 2-in. cubic cell. A cylindrical geometry is currently being implemented for further studies. During simulations of two distinct *m/z* values, a second singly-charged ion of *m/z* 150.0000 is included in a 1:1 ratio to the Cs ion number. Before excitation, the ion cloud is generated as an ellipsoid (major axis 0.2 cm, minor axis 0.05 cm), with the major axis parallel to the magnetic field and a uniform distribution of particles. The initial particle velocity distribution is Maxwellian at 300 K. For each particle, the direction of the velocity vector is randomized. For excitation in the single *m/z* simulations of Cs^+, an on-resonance radiofrequency (rf) burst was utilized. Variation in the excite voltage from 2 to 10 $V_{p\text{-}p}$ resulted in an orbital radius ranging from 15% to 85% of the analyzer cell radius. During simulations of ions with two distinct *m/z* values, a chirp excitation was utilized with voltages ranging from 60 to 180 $V_{p\text{-}p}$ producing orbital radii ranging from 15% to 60%. For each computational experiment, a simulated time domain transient was acquired and a frequency domain spectrum was derived using the fast Fourier transform (FFT) incorporated in FOM-AMOLF's AWE software [26]. Visualization of the simulated ion cloud was accomplished with in-house software developed at FOM-AMOLF [27].

Table 1. Parameters utilized for PIC stimulations and prior experimental data

Simulation	
Trapping potential	1.0 V
Magnetic field	7.0 T
Analyzer geometry	Cubic
Ion cloud	Ellipsoid
Semi-major axis	0.2 cm
Semi-minor axis	0.05 cm
Trap dimension	5.08 cm
PIC grid	32 × 32 × 32
Simulated particles	100–1,000,000
Ion *m/z*	132.9054, 150.0
Excitation	
Voltage	2–180 $V_{p\text{-}p}$
Excitation steps	16383
Duration	90 μs
Time step	0.005 μs/step
Detection	
Detection steps	2097152
Duration	52 ms
Time step	0.024 μs/step
Experimental	
Trapping potential	1.0 V
Magnetic field	7.0 T
Analyzer geometry	Closed-end cylindrical
Detection	
Excitation voltage	100 $V_{p\text{-}p}$
Duration	47.5 ms

Results and Discussion

Contrary to prior published proposals regarding space–charge interaction between ions of the same mass-to-charge [2, 12], experimental results in our lab have demonstrated frequency shifts among monoisotopic populations of Cs^+ ions [13]. A linear decrease in frequency with increasing ion abundance was observed over most of the range of ion abundance, and attributed to space charge-induced frequency shifts between Cs^+ ions. At the lowest ion abundance values that could be measured, an increase in frequency with an increase in ion abundance was observed, suggesting another, yet to be explained, phenomenon. At intermediate ion num-

ber, the observed frequency reaches a maximum, shown in Figure 1. Simulations allow this effect to be examined in systematic fashion by varying parameters such as ion number or radius of the cyclotron orbit.

Simulation Model Validation

Before initiating computational experiments to determine the source of the frequency shifts, a model of the experimental configuration was constructed based on the parameters for the initial data acquisition. One difference limits the direct comparison of our simulation results: the previously published experimental results were acquired on a Bruker FTICR-MS equipped with a close-ended cylindrical cell [28]. For the simulations, we are currently limited to the cubic cell geometry, but are able to apply either a trapping potential for a cubic cell or an idealized quadrupolar potential. The shape of the trapping potential of the close-ended cylindrical cell lies between these two extremes; therefore simulation results were obtained with both trapping electric field geometries, allowing for a reasonable approximation of our experimental configuration.

Ion trajectory simulations performed with a resonance excitation voltage of 4 $V_{p\text{-}p}$, shown in Figure 2, correspond to a final cyclotron radius of ~35% of the analyzer cell radius. For both applied trapping potentials, a nearly linear decrease in calculated cyclotron frequency is observed as the ion number increases. This trend is consistent with the prior experimental results described above. The difference in slope between the two types of trapping potentials can be attributed to variations between exciting an ion into an inhomogeneous cubic trapping potential versus an ideal quadrupolar potential. At low ion numbers, the simulations using either potential both approach the reduced cyclotron frequency. In the case of the cubic potential, a maximum is observed in the plot of observed frequency versus ion number, and a reduction in frequency occurs for decreasing ion number when the number of ions is less than 4000. This feature may be due to a combination of inhomogeneities in the cubic trapping potential and cloud decoherence at low ion number [25]. Ion trajectory visualizations reveal a loss of coherence in the ion cloud near the maxima for the cubic potential, while the cloud maintains coherence in the quadrupolar potential. As we do not fully understand the source of this anomaly in the cubic trapping potential, a quadrupolar potential was chosen for the remainder of our current simulations. This variation will be a source of further study.

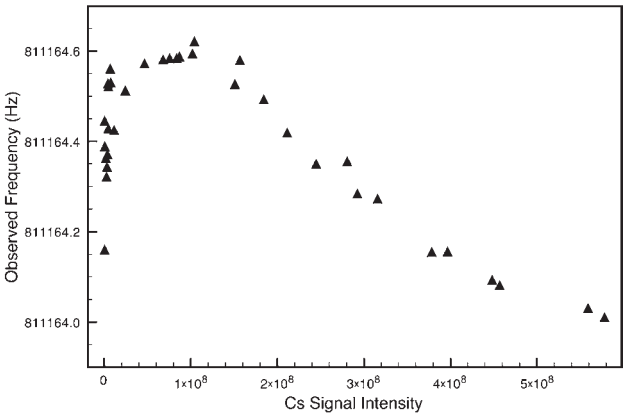

Figure 1. Experimentally observed frequency shifts observed for a monoisotopic Cs^+ population, acquired by varying the concentration of a CsI electrospray solution and ion accumulation time in a storage hexapole before injection into the FTICR analyzer (replotted from data published in reference [13]). Simulated frequencies vary from these experimental frequencies by ~2 kHz because simulations were conducted at exactly 7.0 T, whereas the experimental magnetic field is about 7.02 T.

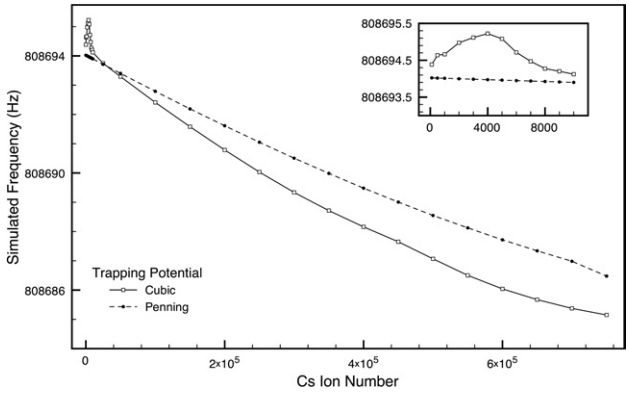

Figure 2. Simulated frequency shifts for a cubic and quadrupolar trapping potential for Cs^+ populations ranging from 100 to 750,000 at 35% cell radius. The inset shows an expansion of the low ion number region of the curve.

Excitation Radius Dependence–Image Charge Interaction Effects

Simulations of varying Cs^+ number were conducted using burst excitation voltages ranging from 2 to 10 $V_{p\text{-}p}$, in increments of 2 V. These applied voltages correspond to orbital radii of ~15%, 35%, 50%, 65%, and 85% of the cell radius. As shown in Figure 3, increasing the excitation radius of a monoisotopic ion population produces an increase in the slope of the plot of the observed frequency shift versus ion number. For a given excitation radius, this frequency shift versus ion number is approximately linear.

Previously, Easterling et al. observed not only a linear correlation between observed frequency and ion number in MALDI FTICR-MS [29] for a group of ions of various mass-to-charge values, but also a decrease in frequency shift with increasing excitation voltage. This experimental result was rationalized as a decrease in ion–ion interactions (space–charge) as the radius of excitation increased; at higher radius, the ion density decreases, thus reducing the frequency shift based on space charge effects between ions of different mass-to-charge. In sharp contrast, for ions of a single mass-to-

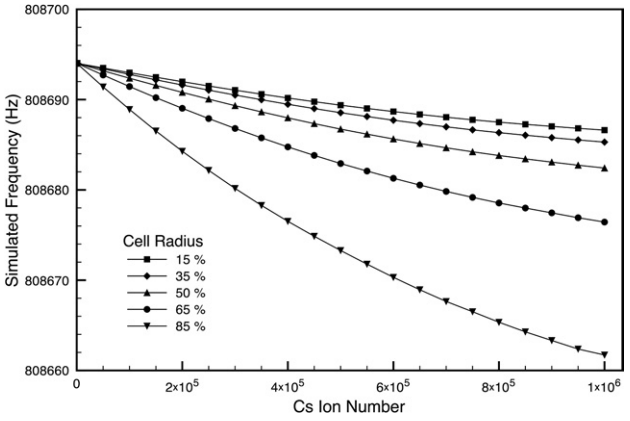

Figure 3. Simulated frequency shifts for ion orbital radii ranging from 15% to 85% of the cell radius for Cs^+ populations ranging from 100 to 1000,000 in a quadrupolar trapping potential.

charge value, the frequency shift from the multiparticle simulations is found to increase in slope with increasing excitation voltage. This result can be attributed to an increase in the interaction between the ions and their image charge as the orbital radius increases, bringing ions closer to the excitation and detection electrodes. In the experimental results with ions of differing *m/z* values present, space–charge effects between ions of different mass-to-charge were significantly larger than the ion–image current interaction, and so the dominating effect observed was that of decreasing space charge with increasing orbital radius. The simulations suggest that there is no space–charge effect on observed frequency for ions of the same mass-to-charge, in agreement with the work of Chen and Comisarow [2]. Thus, the much smaller effect from ion–image charge interactions can be observed, and this is expected to increase with increasing orbital radius.

Marshall and coworkers have previously made analytical calculations of the image charge interaction of a single ion in orthorhombic/cubic and cylindrical geometries as functions of radial and axial position [6]. The calculated frequency shift for a cubic cell was $\sim 1.0 \times 10^{-5}$ Hz per ion for excitation to 50% of the cell radius (1.0 in. cubic cell, 3.0 T magnetic field.) Correcting for the 1/B dependence, this shift becomes 4.29×10^{-6} at 7.0 T. This value is in close agreement with the results of our simulations, where we observe a 1.5×10^{-5} Hz shift per ion in a cubic cell (2.0 in. cubic cell at 7.0 T magnetic field) orbiting at 50% of the cell radius. The analytical solution of the line charge model previously utilized by Gorshkov et al. [5] and Mitchell [24] can also serve as a baseline for comparison. The calculated shift for a single ion in a 2.0 in. cell at 7.0 T is 2.6×10^{-6} Hz. Tinkle and Barlow have also calculated this shift in a cubic cell [30]. For a single ion at 7.0 T (1.6 in. cubic cell), the magnitude of the shift is 2.7×10^{-6} Hz. Allowing for the variations in cell design and ion position for each study, these values are all in good agreement.

There is a slight curvature to the plots in Figure 3, corresponding to frequency shifts that are slightly smaller than one would predict for linear scaling with ion number. Linear scaling is expected if all of the ions were located at the same point in space. As the number of ions increases, coulombic repulsion results in a larger, more diffuse ion cloud and a more diffuse image charge, leading to a small reduction in the ion–image charge interaction. Such behavior was not predicted by the analytical calculations of Marshall or Barlow, as they focused on the behavior of a single ion.

The dependence of the observed frequency on the orbital radius of an ion, shown in Figure 4, also shows good agreement with Marshall's calculations for single ions. The frequency shift increases quadratically as the distance between the ions and the cell plate decreases, as one would expect for the interaction of two point charges. At low ion number, there is a very small shift (<1.0 Hz) as the radius is increased, but this shift increases to several Hz with increasing ion number. For an orbital radius of 50% of the cell radius, the frequency shift is 8 Hz for 10^6 ions, and 14 Hz at an orbital radius of 65% of the cell radius.

Comparison to Interactions Between Ions of Different m/z Values

To further validate the source of the experimentally observed frequency shifts in Cs^+, a series of simulations were conducted in which a second population of singly-charged ions of *m/z* 150 was introduced in a 1:1 ratio to the Cs^+ number. Based on the ability of the PIC code to enable coulombic interactions between particles, space charge effects can be recorded in these calculations. The observed frequency of Cs^+ for three excitation radii is shown in Figure 5, compared with the observed frequency without the addition of an ion of different mass-to-charge. Over the range of ion numbers, 500 to 250,000, the frequency for Cs^+ present by itself decreases by only 3 Hz, whereas the frequency for Cs^+ when ions of a second *m/z* value are present (same total number of ions) decreases by 21 Hz, for an orbital

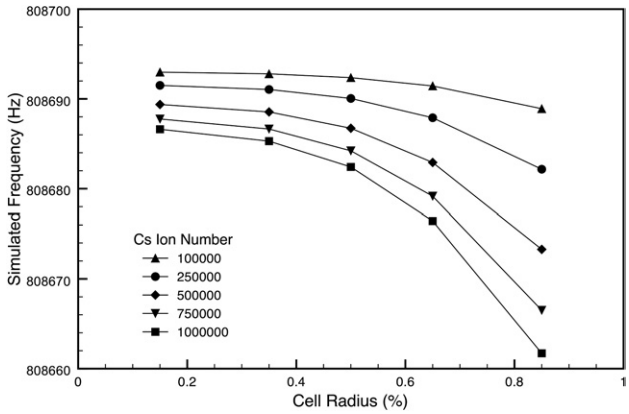

Figure 4. Simulated frequency shifts as a function of orbital radius for selected Cs^+ numbers in a quadrupolar trapping potential.

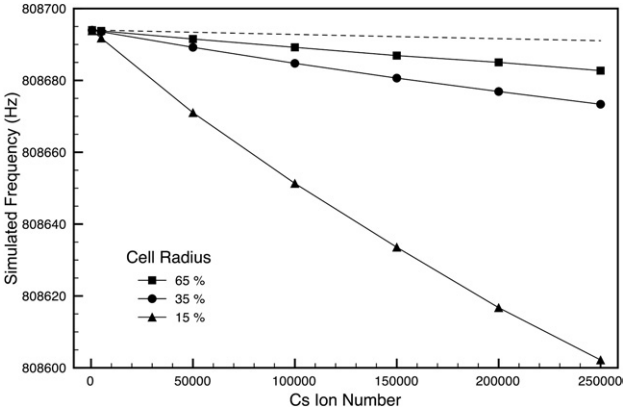

Figure 5. Simulated frequency shifts in Cs^+ when a second ion is added to the FTICR-MS analyzer employing a quadrupolar trapping potential. Orbital radii from 1% to 60% of the cell radius are shown. The dashed line represents the frequency shifts present at 35% cell radius for a population of only Cs^+, for comparison.

radius of 35%. The resulting ratio of the slopes is 1:7, in excellent agreement to the experimental value of 1:7.5 [13]. The much steeper slope of the simulated frequencies for two different mass-to-charge values corresponds to the addition of ion–ion space charge effects to the ion–image charge interaction. Also shown in Figure 5, the previously discussed space charge behavior described by Easterling et al. [29] is also replicated by the simulations. As the excitation radius is increased, the slope of the frequency shift decreases, demonstrating that space–charge interactions between ions of differing mass-to-charge decrease as the orbital radius increases. In contrast, ion–image current interactions increase with increasing orbital radius. For cell designs in which the orbital radius can approach the cell radius, the magnitude of the frequency shift from ion–image charge interactions may approach or exceed that from ion–ion interactions.

Considerations for Mass Calibration

The exact relationship between frequency and mass-to-charge in FTICR-MS depends upon a number of experimental factors, and various calibration laws have been proposed to attain this value with high accuracy by including terms that account for space–charge effects either explicitly or implicitly [11, 29, 31–34]. Muddiman and Oberg have examined several calibration equations, and have proposed a statistically-derived equation that includes terms that can be interpreted as being due to both global and local space–charge [31]. Global space–charge is the general reduction in observed frequency that occurs as a function of the total summed ion abundance, while local space charge is a smaller term that takes into account a reduced interaction between ions of the same mass-to-charge [7, 34]. Based on the work presented here, apparently the latter term in the Muddiman calibration law accounts for ion–image charge interactions. For mass spectra in which the intensity distribution of detected ions is relatively constant over the mass range, the effect of ion–image charge interactions would be negligibly small compared with conventional space–charge interactions. On the other hand, in MS/MS experiments where the precursor intensity is much greater in intensity than the product ions, for example, electron capture dissociation [35] or electron detachment dissociation [36], the image charge induced frequency shift will be significant for the precursor ion, but insignificant for the product ions. For this reason, the precursor ion should not be used for internal calibration or lock-mass calibration, unless the calibration equation accounts explicitly for ion–image charge interactions.

Conclusions

The application of particle-in-cell ion trajectory calculations provides the means to gain insight into the fundamentals of ion behavior in FTICR-MS. Prior experimental results for both like and unlike ions have been explained based on the observed frequency shifts as experimental parameters are varied during simulations, and analytical calculations of image charge-induced frequency shifts for single ions have been validated for ion populations of a size that is typical for real experiments. Space charge-induced shifts can be minimized by exciting to increased cell radius, but image charge based frequency shifts will increase and provide mass errors in FTICR-MS that should be taken into consideration for mass calibration. The close correspondence of the PIC simulation results with prior experiment and theory provides validation for this approach to accurately modeling the interactions of large populations of ions in FTICR-MS [24, 25].

Acknowledgments

F.E.L. and I.J.A. gratefully acknowledge financial support for travel to The Netherlands from PIRE: a U.S.–Dutch Mass Spectrometry Consortium for Advanced Modeling and Biological Structure and Imaging Applications sponsored by the National Science Foundation Office of International Science and Engineering (OISE-730072). F.E.L. also acknowledges Marco Konijnenburg (FOM-AMOLF) for assistance with modifications to the AWE software. E.N. and A.K. acknowledge Gleb Vladimirov (Institute for Energy Problems of Chemical Physics) for his contributions to the development of the PIC code.

References

1. Comisarow, M. B.; Marshall, A. G. Fourier-Transform Ion-Cyclotron Resonance Spectroscopy. *Chem. Phys. Lett.* **1974,** *25*, 282–283.
2. Chen, S. P.; Comisarow, M. B. Simple Physical Models for Coulomb-Induced Frequency Shifts and Coulomb-Induced Inhomogeneous Broadening for Like and Unlike Ions in Fourier Transform Ion Cyclotron Resonance Mass Spectrometry. *Rapid Commun. Mass Spectrom.* **1991,** *5*, 450–455.
3. Chen, S. P.; Comisarow, M. B. Modeling Coulomb Effects in Fourier-Transform Ion Cyclotron Resonance Mass Spectrometry by Charged Disks and Charged Cylinders. *Rapid Commun. Mass Spectrom.* **1992,** *6*, 1–3.
4. Mitchell, D. W.; Smith, R. D. Cyclotron Motion of 2 Coulombically Interacting Ion Clouds with Implications to Fourier-Transform Ion-

Cyclotron Resonance Mass-Spectrometry. *Phy. Rev. E* **1995,** *52*, 4366–4386.
5. Gorshkov, M. V.; Marshall, A. G.; Nikolaev, E. N. Analysis and Elimination of Systematic Errors Originating from Coulomb Mutual Interaction and Image Charge in Fourier Transform Ion Cyclotron Resonance Precise Mass Difference Measurements. *J. Am. Soc. Mass Spectrom.* **1993,** *4*, 855–868.
6. Xiang, X.; Grosshans, P. B.; Marshall, A. G. Image Charge-Induced Ion Cyclotron Orbital Frequency Shift for Orthorhombic and Cylindrical FT-ICR Ion Traps. *Int. J. Mass Spectrom. Ion Processes* **1993,** *125*, 33–43.
7. Masselon, C.; Tolmachev, A. V.; Anderson, G. A.; Harkewicz, R.; Smith, R. D. Mass Measurement Errors Caused by "Local" Frequency Perturbations in FTICR Mass Spectrometry. *J. Am. Soc. Mass Spectrom.* **2002,** *13*, 99–106.
8. Aizikov, K.; O'Connor, P. B. Use of the Filter Diagonalization Method in the Study of Space Charge Related Frequency Modulation in Fourier Transform Ion Cyclotron Resonance Mass Spectrometry. *J. Am. Soc. Mass Spectrom.* **2006,** *17*, 836–843.
9. Aizikov, K.; Mathur, R.; O'Connor, P. B. The Spontaneous Loss of Coherence Catastrophe in Fourier Transform Ion Cyclotron Resonance Mass Spectrometry. *J. Am. Soc. Mass Spectrom.* **2009,** *20*, 247–256.
10. Jeffries, J. B.; Barlow, S. E.; Dunn, G. H. Theory of Space–charge Shift of Ion-Cyclotron Resonance Frequencies. *Int. J. Mass Spectrom. Ion Processes* **1983,** *54*, 169–187.
11. Francl, T. J.; Sherman, M. G.; Hunter, R. L.; Locke, M. J.; Bowers, W. D.; McIver, R. T. Experimental-Determination of the Effects of Space–charge on Ion-Cyclotron Resonance Frequencies. *Int. J. Mass Spectrom. Ion Processes* **1983,** *54*, 189–199.
12. Wineland, D.; Dehmelt, H. Line Shifts and Widths of Axial, Cyclotron and G-2 Resonances in Tailored, Stored Electron (Ion) Cloud. *Int. J. Mass Spectrom. Ion Phys.* **1975,** *16*, 338–342.
13. Wong, R. L.; Amster, I. J. Experimental Evidence for Space–charge Effects Between Ions of the Same Mass-to-Charge in Fourier-Transform Ion Cyclotron Resonance Mass Spectrometry. *Int. J. Mass Spectrom.* **2007,** *265*, 99–105.
14. Dahl, D. A. SIMION for the Personal Computer in Reflection. *Int. J. Mass Spectrom.* **2000,** *200*, 3–25.
15. Hendrickson, C. L., Beu, S. C., Blakney, G. T., Marshall, A. G. SIMION Modeling of Ion Image Charge Detection in Fourier Transform Ion Cyclotron Resonance Mass Spectrometry. *Int. J. Mass Spectrom.* **2009,** *283*, 100–104.
16. Nikolaev, E. N.; Miluchihin, N. V.; Inoue, M. Evolution of an Ion Cloud in a Fourier Transform Ion Cyclotron Resonance Mass Spectrometer During Signal Detection: Its Influence on Spectral Line Shape and Position. *Int. J. Mass Spectrom. Ion Processes* **1995,** *148*, 145–157.
17. Miluchihin, N. V.; Miura, K.; Inoue, M. Application of a Parallel Computer to Simulation of Ion Trajectories in an Ion Cyclotron Resonance Spectrometer. *Rapid Commun. Mass Spectrom.* **1993,** *7*, 966–970.
18. Hockney, R. W.; Eastwood, J. W. Computer Simulation Using Particles; Adam Hilger: New York, 1988; pp 1–42.
19. Birdsall, C. K. Particle-In-Cell Charged-Particle Simulations, Plus Monte-Carlo Collisions With Neutral Atoms, PIC-MCC. *IEEE Trans. Plasma Sci.* **1991,** *19*, 65–85.
20. Peratt, A. L. Advances in Numerical Modeling of Astrophysical and Space Plasmas. *Astrophys. Space Sci.* **1996,** *242*, 93–163.
21. Dawson, J. M. Particle Simulation of Plasmas. *Rev. Mod. Phys.* **1983,** *55*, 403–447.
22. Birdsall, C. K.; Langdon, A. B. Plasma Physics via Computer Simulation; McGraw-Hill: New York, 1985; pp 55–75.
23. Mitchell, D. W.; Smith, R. D. Two-Dimensional Many Particle Simulation of Trapped Ions. *Int. J. Mass Spectrom.* **1997,** *165*, 271–297.
24. Mitchell, D. W. Realistic Simulation of the Ion Cyclotron Resonance Mass Spectrometer Using A Distributed Three-Dimensional Particle-In-Cell Code. *J. Am. Soc. Mass Spectrom.* **1999,** *10*, 136–152.
25. Nikolaev, E. N.; Heeren, R. M. A.; Popov, A. M.; Pozdneev, A. V.; Chingin, K. S. Realistic Modeling of Ion Cloud Motion in a Fourier Transform Ion Cyclotron Resonance Cell by Use of a Particle-In-Cell Approach. *Rapid Commun. Mass Spectrom.* **2007,** *21*, 3527–3546.
26. Mize, T. H.; Taban, I.; Duursma, M.; Seynen, M.; Konijnenburg, M.; Vijftigschild, A.; Doornik, C. V.; Rooij, G. V.; Heeren, R. M. A. A Modular Data and Control System to Improve Sensitivity, Selectivity, Speed of Analysis, Ease of Use, and Transient Duration in an External Source FTICR-MS. *Int. J. Mass Spectrom.* **2004,** *235*, 243–253.
27. Burakiewicz, W.; van Liere, R. Analyzing Complex FTMS Simulations: A Case Study in High-Level Visualization of Ion Motions. *IEEE Trans. Vis. Comput. Graphics* **2006,** *12*, 1037–1043.
28. Caravatti, P.; Allemann, M. The Infinity Cell - A New Trapped-Ion Cell with Radiofrequency Covered Trapping Electrodes for Fourier-Transform Ion-Cyclotron Resonance Mass-Spectrometry. *Org. Mass Spectrom.* **1991,** *26*, 514–518.
29. Easterling, M. L.; Mize, T. H.; Amster, I. J. Routine Part-Per-Million Mass Accuracy for High-Mass Ions: Space–charge Effects in MALDI FT-ICR. *Anal. Chem.* **1999,** *71*, 624–632.
30. Tinkle, M. D.; Barlow, S. E. Image Charge Forces Inside Conducting Boundaries. *J. Appl. Phys.* **2001,** *90*, 1612–1624.
31. Muddiman, D. C.; Oberg, A. L. Statistical Evaluation of Internal and External Mass Calibration Laws Utilized in Fourier Transform Ion Cyclotron Resonance Mass Spectrometry. *Anal. Chem.* **2005,** *77*, 2406–2414.
32. Ledford, E. B.; Rempel, D. L.; Gross, M. L. Space Charge Effects in Fourier Transform Mass Spectrometry. II. Mass Calibration. *Anal. Chem.* **1984,** *56*, 2744–2748.
33. Li-Kang, Z.; Don, R.; Birendra, N. P.; Michael, L. G. Accurate Mass Measurements by Fourier Transform Mass Spectrometry. *Mass Spectrom. Rev.* **2005,** *24*, 286–309.
34. Burton, R. D.; Matuszak, K. P.; Watson, C. H.; Eyler, J. R. Exact Mass Measurements Using a 7 Tesla Fourier Transform Ion Cyclotron Resonance Mass Spectrometer in a Good Laboratory Practices-Regulated Environment. *J. Am. Soc. Mass Spectrom.* **1999,** *10*, 1291–1297.
35. Zubarev, R. A.; Kelleher, N. L.; McLafferty, F. W. Electron Capture Dissociation of Multiply Charged Protein Cations. A Nonergodic Process. *J. Am. Chem. Soc.* **1998,** *120*, 3265–3266.
36. Wolff, J. J.; Amster, I. J.; Chi, L.; Linhardt, R. J. Electron Detachment Dissociation of Glycosaminoglycan Tetrasaccharides. *J. Am. Soc. Mass Spectrom.* **2007,** *18*, 234–244.